ChemPubSoc Europe

DOI: 10.1002/chem.201500473

CHEMISTRY
A European Journal
Full Paper

Molecular Dynamics |Hot Paper|

Complex Reaction Environments and Competing Reaction Mechanisms in Zeolite Catalysis: Insights from Advanced Molecular Dynamics

Kristof De Wispelaere,[a, b] Bernd Ensing,*[b] An Ghysels,[a] Evert Jan Meijer,[b] and Veronique Van Speybroeck*[a]

Abstract: The methanol-to-olefin process is a showcase example of complex zeolite-catalyzed chemistry. At real operating conditions, many factors affect the reactivity, such as framework flexibility, adsorption of various guest molecules, and competitive reaction pathways. In this study, the strength of first principle molecular dynamics techniques to capture this complexity is shown by means of two case studies. Firstly, the adsorption behavior of methanol and water in H-SAPO-34 at 350 °C is investigated. Hereby an important degree of framework flexibility and proton mobility was observed. Secondly, the methylation of benzene by methanol through a competitive direct and stepwise pathway in the AFI topology was studied. Both case studies clearly show that a first-principle molecular dynamics approach enables unprecedented insights into zeolite-catalyzed reactions at the nanometer scale to be obtained.

Introduction

Chemical conversions in zeolites play an essential role in today's industrial catalysis.[1–3] Within the field of heterogeneous catalysis, the conversion of methanol to hydrocarbons (MTH) or olefins (MTO) over acidic zeolites has received a lot of attention over the last decades because of its relevance in the search for alternative processes to produce hydrocarbon products.[4–7] The MTO process has been developed experimentally in the past 3–4 decades and is currently being industrialized.[5] Methanol can be obtained from coal, natural gas, or biomass, and is in turn converted into ethene, propene, or other hydrocarbons. The process proved extremely difficult to unravel at the nanoscale level because of various factors such as pressure, temperature, and the occurrence of competing reaction mechanisms, which highly influence the catalytic performance of the system. Due to its complexity, it is a very challenging case study for theoretical modeling studies.[8]

Currently, there is a consensus that a hydrocarbon pool (HP) mechanism operates during the methanol conversion process. Herein, an organic center is trapped in the zeolite pores and acts as a co-catalyst.[9–11] The HP may be of aromatic or aliphatic nature and the two corresponding types of catalytic cycles are in close connection with each other, a concept that is called the dual cycle.[12] Depending on the catalyst topology and operating conditions, either one or both cycles may be responsible for olefin formation during the methanol conversion process.[12–14]

Theoretical contributions have proven to be indispensable within MTO research. Methodological developments and a steady increase in computer power contributed to the fact that many properties, in particular rate coefficients of well-defined elementary reactions, are now routinely calculated with high accuracy.[8,15–17] However, theoretical chemists are still confronted with paramount challenges to thoroughly explain experimental observations. The true challenge lies in linking the model system with experimental or industrial conditions. Weckhuysen nicely illustrated, in his review on spatial heterogeneities in catalytic solids at different length and time scales, that the observed function of a material is the result of a multiscale nature of phenomena.[18] Even when focus is set on phenomena occurring in the nanometer range of the active site, routinely applied static methods to study chemical reactions are often insufficient to mimic operational conditions. A first complication is that on complex potential energy surfaces (PES), typically many isoenergetic configurations occur. To properly describe the complexity of such processes, one must study the free energy surface (FES).[19] A schematic representation of a hypothetical FES in terms of two reaction coordinate variables is shown in Figure 1. It is clear that two minima on the surface can be connected by various competitive reaction paths as hypothetically illustrated in Figure 1. Reactant A and product B are connected by direct reaction paths and a two-

[a] K. De Wispelaere, Prof. Dr. A. Ghysels, Prof. Dr. V. Van Speybroeck
Center for Molecular Modeling (CMM)
Ghent University, Technologiepark 903, 9052 Zwijnaarde (Belgium)
E-mail: veronique.vanspeybroeck@ugent.be

[b] K. De Wispelaere, Dr. B. Ensing, Prof. Dr. E. J. Meijer
Amsterdam Center for Multiscale Modeling and
van 't Hoff Institute for Molecular Sciences
University of Amsterdam, Science Park 904
1098 XH Amsterdam (The Netherlands)
E-mail: b.ensing@uva.nl

Supporting information for this article is available on the WWW under http://dx.doi.org/10.1002/chem.201500473.

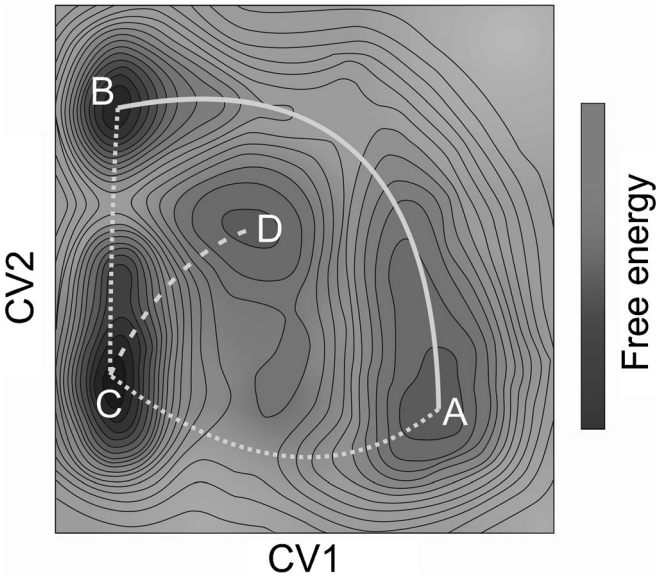

Figure 1. Hypothetical two dimensional free energy surface as a function of two collective variables. Minima A and B are connected by a direct and a two-step reaction path. Intermediate C can also lead to byproduct D.

step mechanism via intermediate C. Additionally, intermediate C can form the byproduct D. Bell and co-workers recently demonstrated that 0 K potential energy surfaces alone cannot accurately predict product selectivities because selectivity in zeolite catalysis is largely determined by dynamical effects in high-temperature reaction pathways.[19,20] A second issue is that various guest molecules can be present in the pores of the material, and each of them can play an active role during the chemical conversions. The loading and role of these additional guest molecules typically depend on the operating conditions, such as temperature and pressure. More guest molecules introduce more degrees of freedom in the system, making it more difficult to set up accurate static models. A third complication concerns the zeolite framework flexibility, which may impact the conversions it catalyzes. Every zeolite topology exhibits a flexibility window as theoretically demonstrated by Kapko and coworkers.[21] It was observed that gas molecules with a Lennard–Jones diameter larger than the time-averaged narrow sodalite windows can diffuse through the sodalite zeolite due to the framework flexibility.[22,23] Also, the flexibility of any bulky reaction intermediate implies a significant increase in conformational degrees of freedom that should be appropriately accounted for.[24]

In this paper we apply advanced molecular dynamics techniques, which, to some extent, allow us to capture the framework flexibility, the presence of guest molecules, and the occurrence of competitive reaction paths. This is done by means of two case studies, which are inspired by the MTO process. The first case sheds light on proton mobility in water or methanol occluded in the CHA cages of the industrially relevant MTO catalyst H-SAPO-34.[25] For Brønsted acid-catalyzed reactions, proton mobility is essential because proton transfer is the first step in the activation of reactants. Additionally, the influence of the guest molecule loading on the flexibility of the H-SAPO-34 framework will be discussed. The second case study focusses on the accurate simulation of competitive pathways by using the metadynamics approach. Therefore, the methylation of benzene by two methanol molecules in H-SSZ-24 is selected. As shown earlier, methylation reactions are crucial steps in the HP mechanism of the MTO process.[5,6,26] There is still an ongoing debate about the exact reaction mechanism, for which two possible reaction routes have been proposed.[26] On the one hand, the methylation can occur in a concerted fashion, meaning that protonation of methanol, water formation, and the methyl transfer occur simultaneously. On the other hand, there is the stepwise mechanism in which methanol protonation, water formation, and the formation of a framework bound methoxide occur prior to the actual methylation. The relative importance of the direct and the stepwise mechanism during the methylation of benzene in H-SSZ-24 will be assessed by applying a dynamical approach, capturing both pathways in one simulation.

Currently, a thorough exploration of the FES is not routinely applied in zeolite-catalyzed chemistry because there are still a lot of methodological hurdles to overcome. These are typically related to the wide range of characteristic time scales associated with a molecular system in zeolite catalysis. More specifically, to simulate a chemical reaction, special techniques have to be applied for sampling the less probable regions on the FES that are inherently related with an activated process.[27–37] Only a limited number of studies have applied techniques that go beyond the static approach to describe chemical transformation in zeolites.[19,20,38–44] The strength of a dynamical approach was earlier demonstrated by some of the present authors. We reported that the influence of the presence of multiple protic molecules on the methylation of benzene[44] and methoxide formation[42] in H-ZSM-5 has to be studied with molecular dynamics. These studies demonstrated that formation of protonated clusters of protic molecules has to be taken into account when modeling reactions under conditions of high reactant loadings, in particular in case of protic reactants that can play a solvent-like role.

Results and Discussion

In this paper, results from ab initio molecular dynamics (AIMD) and metadynamics (MTD) simulations are presented. Therefore, density functional theory (DFT) calculations were applied to periodic catalyst models of H-SAPO-34 and H-SSZ-24, which accurately account for the topology and flexibility of the materials. This approach is in contrast with the often adopted finite cluster models, wherein only a fraction of the material is accounted for.[8] The chabazite (CHA)-structured H-SAPO-34 is characterized by large elliptic cages, connected by narrow 8-ring windows (3.8×3.8 Å), whereas the AFI-structured H-SSZ-24 exhibits large one-dimensional pores consisting of 12-rings (7.3×7.3 Å; Figure 2). Recently, both catalysts have been studied experimentally.[13,45,46] H-SAPO-34 is an industrially relevant MTO catalyst,[25] whereas H-SSZ-24 has been studied as a model system because it allows co-feeding studies with bulky aromatic reaction intermediates.[13,43] It was demonstrat-

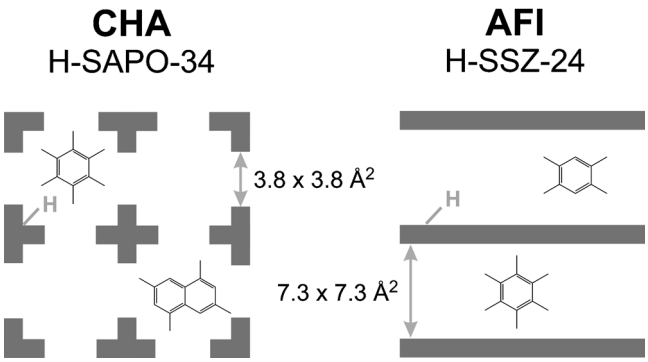

Figure 2. Schematic representation of the CHA-structured H-SAPO-34 and AFI-structured H-SSZ-24 catalysts, with indication of the acid site, the size of the pore opening (taken from the IZA database),[49] and the dominant hydrocarbon pool species during methanol conversion.

ed that in both catalysts, aromatic hydrocarbon pool compounds play a major role during olefin formation.[13,43,47,48]

Case study I: adsorption behavior of methanol or water in H-SAPO-34 at 350 °C

Framework flexibility

The adsorption of methanol and water in several zeolitic materials has been the subject of numerous studies.[50–61] Water and methanol are two crucial molecules during the MTO process. In some cases, water is added to the methanol feed in the form of process condensate or steam to tune the product selectivity.[62,63] MD simulations of H-SAPO-34 loaded with methanol (1, 3, 4, or 5 methanol molecules per acid site) or water (1, 4, 5, 6, 7, or 8 water molecules per acid site) at 350 °C and 1 bar were performed in the NPT ensemble for 50 ps. The applied H-SAPO-34 unit cell contains two acid sites, located in the same 8-ring that connects two CHA cages (the Supporting Information, Figure S1.1). The NPT simulations with a fully flexible unit cell also allow, next to a study of proton mobility, a detailed investigation of the lattice flexibility in terms of various loadings of methanol or water at finite temperatures. Note that cell optimizations at 0 K would not yield reliable data with respect to the cell volume because zeolite and zeotype materials exhibit negative thermal expansion behavior.[64,65] The time-averaged cell lengths are reported in Table S1.1 (the Supporting Information).

We observe that the time-averaged unit cell volume increases upon adsorption of more methanol molecules, indicating that the resulting hydrogen-bonded methanol molecules require more space in the CHA cage (Figure 3). Additionally, the volume expansion appears to be anisotropic as shown in the right panel of Figure 3, showing the maximum expansion and contraction of the H-SAPO-34 unit cell along the three cell vectors with different loadings of the methanol and water molecules. The maximum volume change of 1.6% is mainly due to a relatively high flexibility of the framework in the *c* axis (2% expansion, Figure 3, and the Supporting Information, Figure S2.1). During water adsorption, the time-averaged unit cell

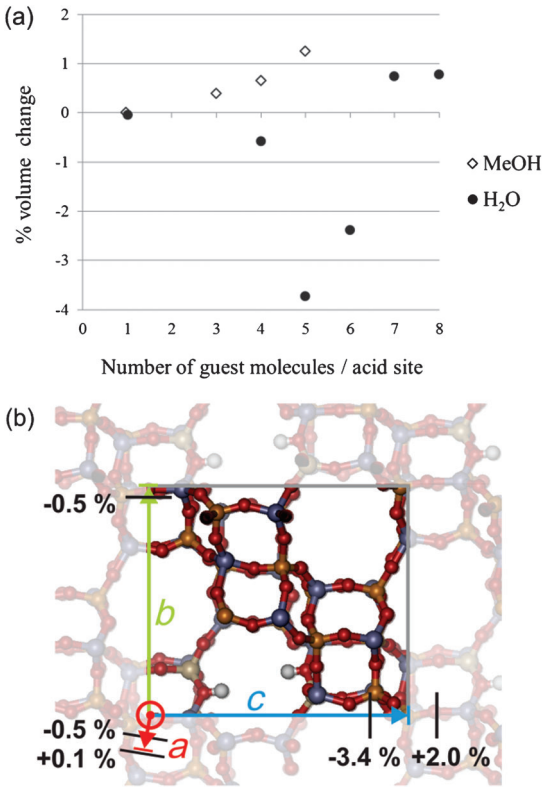

Figure 3. a) Volume change (%) at 350 °C of the H-SAPO-34 framework with two acid sites as a function of the number of adsorbed methanol or water molecules per acid site. b) H-SAPO-34 unit cell (gray box) with two acid sites and indication of the maximum shortening and elongation of the three cell lengths (*a*,*b*,*c*) upon adsorption of multiple methanol or water molecules with respect to the framework loaded with one methanol or water molecule per acid site. All data with respect to the framework loaded with one methanol or water molecule per acid site.

volume first decreases, reaches a minimum at a loading of five water molecules per acid site and then increases upon adsorption of higher loadings (Figure 3). The contraction of the framework is in stark contrast with what is observed for methanol adsorption and clearly shows that the relatively strong interactions of small water molecules with the framework are able to contract the unit cell. Again, the largest framework deformations are situated in the *c* direction (3.4% contraction, Figure 3 and the Supporting Information, Figure S2.1). During adsorption experiments of methanol and water in H-SAPO-34 performed at room temperature, Wragg and co-workers also observed a volume expansion (+0.5%) and contraction (−2%) during methanol and water adsorption, respectively.[66] However, at room temperature the volume change was rather isotropic. The simulations presented here point out that at high temperature, framework expansion, and contraction is highly anisotropic as it preferably occurs in the *c*-direction. This is in line with the experimentally observed 3% increase in the *c*-direction of H-SAPO-34 crystals under MTO conditions and at high temperature (500 °C), during the coking phase.[67–69] These findings illustrate the complexity of accurately taking into account framework flexibility,[70] as anisotropic effects might be at play.

Proton mobility

For Brønsted acid-catalyzed reactions, proton transfers are the essential first steps in the activation of reactants. Earlier spectroscopic and theoretical studies reported proton transfer and mobility in zeolites, depending on the loading of protic molecules like methanol and water in the pores.[51,52,57,71–73] This phenomenon not only plays a role during adsorption, but also affects the catalytic performance in elementary reaction steps. As an example, we mention the role of assisting water molecules on a recently proposed reaction cycle for olefin elimination during methanol conversion in H-SAPO-34.[74] That protic molecules affect proton transfer and possibly also reaction mechanisms can be well understood by the application of dynamical methods, as was already proven for chemical reactions in aqueous solution[75] and zeolites.[42,44] Whether methanol and water form ion pairs upon adsorption in H-SAPO-34 is a point of discussion in the literature and seems to depend on the applied conditions.[50,54,55,58] Furthermore, extensive work was performed by Krishna and co-workers on the effect of hydrogen bonding on adsorption of water–alcohol mixtures in zeolites and the consequences for the diffusivities.[76]

To obtain deeper insights into the mobility of protons in the zeolitic system under study, a profound analysis of the performed MD simulations with varying loadings of methanol or water in H-SAPO-34 was performed. The positions of the protons and all hydrogen atoms in the system were traced during the 50 ps NPT simulations of H-SAPO-34, loaded with different amounts of methanol (1, 3, 4, or 5 molecules per acid site) or water (1, 4, 5, 6, 7, or 8 molecules per acid site), to detect proton transfer. From the MD trajectories, the probability that at least one of the two acid sites in the unit cell of H-SAPO-34 deprotonates, was calculated. The framework is considered to be deprotonated when the shortest distance between the zeolite oxygen atoms surrounding the substitutional defect and all hydrogen atoms exceeds 1.2 Å. The calculated probabilities for framework deprotonation are displayed in Figure 4. For low methanol or water loadings, no framework deprotonation occurs, although a significant elongation of the zeolitic O–H bond is observed at 350 °C. With increasing methanol or water loadings, the probability for framework deprotonation significantly increases. For five methanol molecules per acid site, the probability reaches nearly 100%, indicating that at these conditions at least one methoxonium ion is present in the pores. For water, which has a lower proton affinity than methanol (697 vs. 761 kJ mol^{-1}),[77] higher loadings are required to obtain similar levels of proton transfer. With sufficient amounts of water, hydronium ions can be stable species, which is in correspondence with the findings of Smith et al and Termath et al.[54,55]

Figure 4 showed a high probability for framework deprotonation for H-SAPO-34 loaded with five methanol or eight water molecules per acid site. Although these loadings might seem relatively high, the adsorbed guest molecules are still very mobile under the simulated conditions (the Supporting Information, Section S3). We selected these two most extreme situations for further analysis of proton motion because the best sampling of proton transfer reactions was achieved during these simulations. Note that Figure 4 suggested that also at lower loadings, proton transfer reactions might be important.

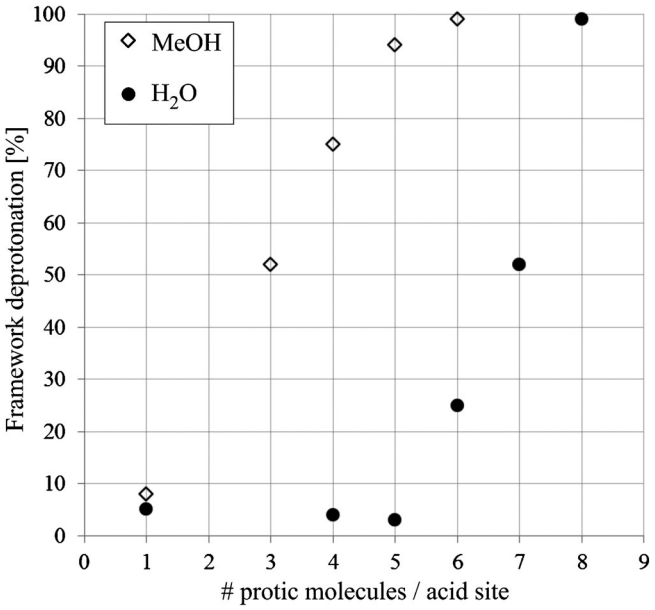

Figure 4. Probability that at least one of the two acid sites in de H-SAPO-34 is deprotonated during a 50 ps MD simulation at 350 °C as a function of the number of adsorbed methanol or water molecules per acid site. Deprotonation occurs when the shortest zeolite oxygen–hydrogen distance exceeds 1.2 Å.

The dots in Figure 5a show the trajectory of a proton (blue) originally located on an acid site and an oxygen atom trajectory (red) of the methanol molecule with which the acidic proton was initially interacting during a simulation of five methanol molecules per acid site in H-SAPO-34 at 350 °C. Apparently, the traced methanol molecule is not able to leave the chabazite cage during the simulation time, whereas the proton is able to diffuse through the 8-ring containing the substitutional defects. Figure 5c shows the displacement of the proton and methanol oxygen atom with respect to their initial positions. Initially both move simultaneously, however, after a couple of picoseconds, proton transfers occur as both atoms no longer move simultaneously.

The right panel of Figure 5 displays the analogue for eight water molecules per acid site in H-SAPO-34 at 350 °C. Again, a proton is able to cross an 8-ring connecting two adjacent chabazite cages (Figure 5b). Figure 5d illustrates that a proton originating from the framework and a water molecule with which the proton was initially interacting, do not move simultaneously throughout the entire simulation, indicating that proton transfer reactions take place between the framework and water molecules. Furthermore, the larger displacements reflect a higher mobility of protons and water molecules compared with those of bulkier methanol molecules.

Our simulations also indicate that framework deprotonation at 350 °C is a highly dynamical process, as the transitions between states with 2, 1, or 0 protonated acid sites in the H-SAPO-34 unit cell loaded with sufficient amounts of methanol

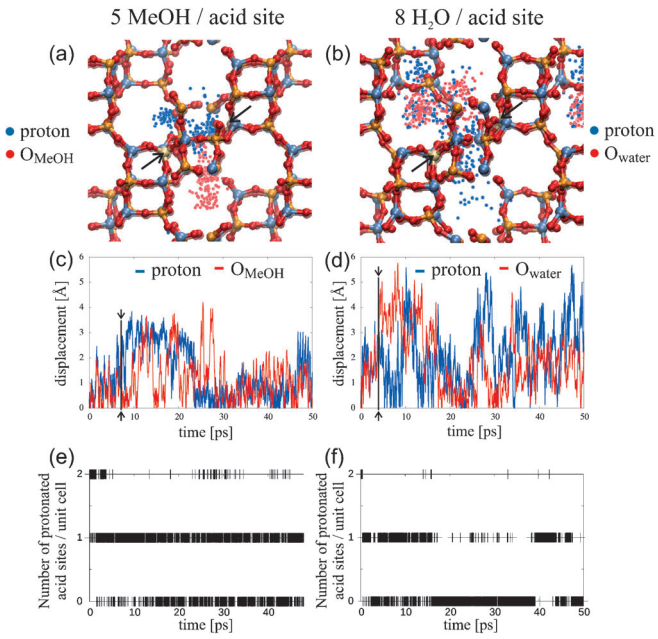

Figure 5. Trajectory and displacement with respect to the atom's initial position of a proton (blue) and a methanol or water oxygen atom (red) during a 50 ps MD simulation of five methanol molecules (a,c) or eight water molecules (b,d) per acid site in H-SAPO-34 respectively; e,f) time evolution of the number of protonated acid sites in the H-SAPO-34 unit cell with two acid sites loaded with five methanol molecules or eight water molecules per acid site. The black arrows in (a,b) indicate the positions of the substitutional defects.

or water are relatively fast (Figure 5 e and f). These fast transitions during regular MD simulations indicate that the corresponding free energy barriers are in the order of *RT*, with *R* being the universal gas constant. Note that the low occupancy of states with two protonated acid sites corresponds with the nearly 100% probability for framework deprotonation shown in Figure 4. The significant probability to find one protonated acid site suggests that an equilibrium between the protonated and deprotonated sites in the zeolite loaded with water or methanol exists. This implies that an acid-catalyzed reaction can occur at the acid site, as well as at a certain distance from it due to proton mobility. Indeed, after framework deprotonation, protons can apparently be located at reasonable distances from their original position at the acid site (the Supporting Information, Figures S4.1 and S4.2). The observation that protic molecules can detach the protons from Brønsted acid sites has consequences on catalytic reactions occurring in the pores. The effect of this phenomenon on activation barriers was recently demonstrated by some of the present authors.[42,44] For the methylation of benzene in H-ZSM-5 it was found that after framework deprotonation, protonated hydrogen-bonded methanol clusters are formed, which are less reactive towards methylation than single protonated methanol molecules. These protonated clusters of protic molecules could be observed as well during our simulations (the Supporting Information, Table S5.1). In the simulation with 8 water molecules per acid site, larger clusters are being formed compared to 5 methanol molecules per acid site.

Free energies and diffusion of protons

Next, free energy profiles were constructed for proton motion through the 8-rings. Therefore, an axis (ξ) is defined perpendicular to the ring plane (Figure 6), and the ξ coordinate is computed for each atom along the trajectory by projecting its coordinates onto this axis. The histogram of ξ coordinates P(ξ) gives the free energy profile:

$$G(\xi) = -\frac{1}{\beta}\ln P(\xi) \quad (1)$$

in which $\beta = 1/k_B T$ and k_B represents the Boltzmann constant. In addition, 8-ring crossing can be detected, because a ring crossing is accompanied by a change in sign of ξ between subsequent trajectory snapshots. Given the free energy profile, a free energy barrier $\Delta G^{\ddagger}$ is conveniently computed from the probability density at the top of the barrier relative to the reactant state probability:

$$\Delta G^{\ddagger} = -\frac{1}{\beta}\ln\frac{\exp[-\beta G(\mathrm{TS})]}{\int_{-\infty}^{\mathrm{TS}}\exp[-\beta G(s)]\mathrm{d}s} \quad (2)$$

in which TS is the position at the top of the barrier along the normalized reaction coordinate (*s*). Statistical error bars on $\Delta G^{\ddagger}$ were computed by repeating the analysis on different data subsets of the entire simulation. Note that the reported error bars do not include the intrinsic errors of the applied methods.

In the simulation with five methanol molecules per acid site, none of the carbon atoms succeeded to cross the 8-ring,

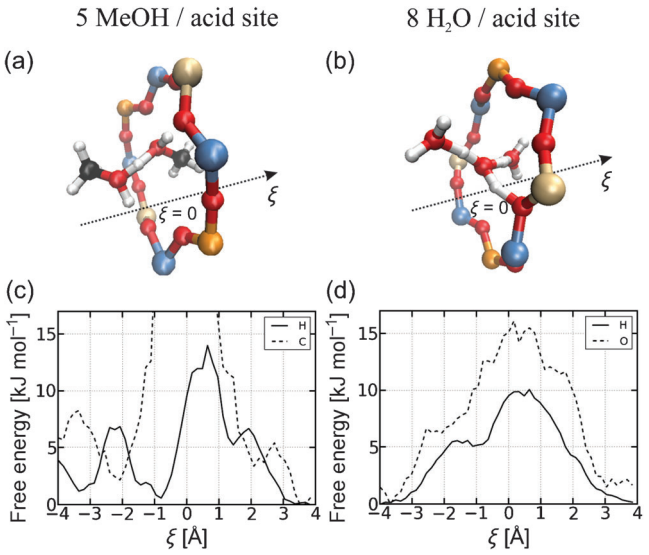

Figure 6. Snapshot of an MD simulation at 350 °C of H-SAPO-34 loaded with five methanol (a) or eight water (b) molecules per acid site, showing proton transfer through an 8-ring through a hydrogen-bonded network, including free energy profile for diffusion of a carbon and hydrogen (c) or oxygen and hydrogen atom (d) through the 8-ring.

whereas the set of 12 hydrogen atoms (originating from the methanol hydroxyl groups and the acid sites) cross in total 180 times, showing the fairly good statistics on these crossings (the Supporting Information, Figures S6.1 and S6.2). These ring crossings of protons proceed exclusively through a Grotthuss-like mechanism involving proton transfer reactions as shown in Figure 6a. Note that both the oxygen atoms surrounding the acid sites and methanol participate as proton donor and acceptor during the proton transfer reaction. Methanol molecules cannot cross the narrow 8-ring during the simulation time, which is reflected by a peak in the free energy profile around the ring position (Figure 6c). Proton transfer through the 8-ring at 350 °C exhibits a free energy barrier of (11 ± 4) kJ mol^{-1}, indicating that this is a relatively easy process at high temperatures. Moreover, due to the relatively high mobility of methanol molecules inside the chabazite cages at 350 °C, methanol can act as a proton vehicle inside one chabazite cage as well. Both mechanisms were earlier proposed for proton motion in solid materials.[72,78] It can be observed that the obtained free energy profile is asymmetrical with respect to the location of the 8-ring. The additional peaks in the free energy profiles of hydrogen (around ξ values of -2.2 Å) and carbon (around ξ values of -4.5 Å) for methanol diffusion through the 8-ring (Figure 6c) could be ascribed to the presence of a large protonated methanol cluster at one side of the ring.

In the simulation with eight water molecules per acid site in H-SAPO-34, the set of 34 hydrogens (originating from the 16 water molecules and 2 acid sites) cross 366 times in total. Unlike methanol, the smaller water molecules do have the capability to cross the narrow 8-rings, with a free energy barrier of (11 ± 2) kJ mol^{-1} (Figure 6d). On the other hand, individual protons can migrate through the 8-ring through a Grotthuss-like mechanism when a hydrogen-bonded network is formed through the 8-ring (Figure 6b). These findings support the hypothesis that proton mobility through the 8-ring occurs in two ways, either by a vehicle mechanism, or by a Grotthuss-like mechanism. The corresponding overall free energy barrier is (7 ± 1) kJ mol^{-1}, indicating a slightly higher proton mobility in water relative to methanol adsorbed in H-SAPO-34 as studied here. Note that detailed descriptions of the Grotthuss mechanism, or revisited versions of it[79] and the proton vehicle mechanism are beyond the scope of this article. Despite the good statistics of the ring crossings, our relatively short simulation times (50 ps) do not allow the accurate calculation of diffusion coefficients.

In summary, this case study shows that adsorption of sufficient amounts of water or methanol induces a relatively high degree of mobility of the acidic protons that were initially located on the acid sites. Once framework deprotonation occurred, a plethora of configurations is sampled. A protonated hydrogen-bonded cluster of methanol or water is formed and broken and the positive charge can be found at a considerable distance from the acid site. Consequently, a static approach would not offer enough sampling to capture all the information reported in this case study. Furthermore, the fast proton motion at 350 °C can be observed during a 50 ps MD simulation, whereas diffusion of small hydrocarbons in 8-ring zeolites typically requires simulations of 10 to 100 ns to obtain sufficient sampling.[80,81] This indicates that proton diffusion occurs on smaller time scales and thus occurs before any highly activated chemical reaction can take place. Hence, this highly dynamical phenomenon has to be taken into account when modeling zeolite-catalyzed reaction steps, since a chemical reaction consequently not necessarily occurs at the catalyst's acid site when a significant amount of protic molecules is present in the pores.

Case study II: simulating competing pathways for benzene methylation in H-SSZ-24

Methylation reactions are crucial steps during methanol conversion because they initiate all hydrocarbon pool reaction cycles proposed so far.[6] Consequently, numerous studies focused on the methylation by methanol, dimethyl ether, or methoxides of aromatics and alkenes in the framework of the MTO process.[16,17,26,42,44,46,82,83] It should be mentioned that the static approach with finite cluster models as applied in most of these studies has been very successful in reproducing and predicting experimentally measured kinetic data.[16,17] However, a similar approach is not applicable for the study of methylation reactions in the large pore AFI-structured H-SSZ-24 as will be demonstrated in this case study. Firstly, the AFI topology exhibits large one-dimensional channels, which are difficult to describe accurately by a finite cluster. Hence, a periodic zeolite model is recommended for this type of material. Secondly, it was shown recently that these systems typically exhibit complex potential energy surfaces that cannot be fully captured by static geometry optimizations.[43] Indeed, due to the large available space inside the channels, guest molecules may adopt many configurations, making it difficult to describe reactions with one pre-reactive complex and transition state.

During a regular molecular dynamics simulation, barriers of approximately RT, in which R is the universal gas constant, can easily be overcome, allowing a good sampling of lowly activated reactions such as the proton transfers discussed in the first case study. However, typical reaction steps occurring in MTO catalytic cycles exhibit free energy barriers of a couple of tens of kJ mol^{-1}.[74,84] As such, these reaction steps are rare events and their probability of occurring during a standard AIMD simulation is relatively low. To enhance sampling of interesting regions on the FES, a multitude of methods have been developed,[37,85,86] among which the metadynamics method, developed by Laio and Parrinello,[34,35,87–90] is very promising to study zeolite-catalyzed reactions.[42,44] The method is especially suited to explore new reaction pathways by identifying a set of collective variables (CVs) that allow sampling interesting regions of the potential and free energy surface. Along these CVs, the free energy landscape is "filled up" with Gaussian-shaped bias potentials to accelerate sampling of rare events (the Supporting Information, Figure S7.1). Afterwards the sum of the Gaussian potentials can be used to reconstruct the FES. For the simulation of chemical reactions, it is especially useful to use coordination numbers as CVs.[42,44]To reconstruct the free energy

surface (FES) after a MTD simulation, the methodology as used in references[44] and[88] were applied as will be further discussed. Free energy barriers were computed according to Equation (2).

Properly defining collective variables is not a straightforward task, because they need to capture the reaction coordinate that leads the system from one energy basin to another. Hence, the reaction coordinate and thus the reaction mechanism have to be known a priori.

In this case study, we investigate the methylation of benzene in H-SSZ-24 at 350 °C with two methanol molecules by the metadynamics technique. Initially, an AIMD simulation of the 1×1×2 H-SSZ-24 supercell (the Supporting Information, Figure S8.1) containing one acid site and loaded with benzene and two methanol molecules was performed in the NPT ensemble at 350 °C and 1 bar to determine the time-averaged cell lengths (the Supporting Information, Table S8.1) and investigate the behavior of the reactants in the pore. With the same criterion as applied in the first case study, we find that the probability for framework deprotonation by the two methanol molecules under the given conditions is 21 %. We observe that the proton can be located at a reasonable distance from the framework (the Supporting Information, Figure S9.1). Furthermore, we calculated that there is a probability of 82 % to find methanol in a dimer conformation. Consequently, it is expected that proton mobility will affect the methylation reaction as the reaction can start from physisorbed methanol, a single protonated methanol molecules, or protonated methanol dimers.

To avoid the assumption of a concerted or a stepwise methylation mechanism, three CVs were defined as displayed in Figure 7: One coordination number to describe the methanol

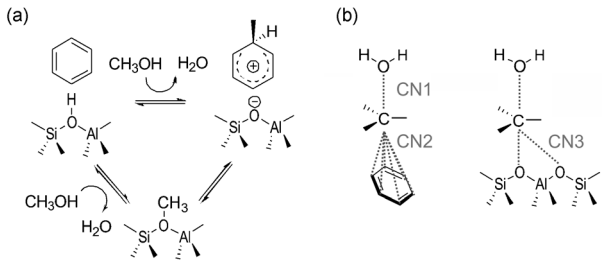

Figure 7. a) The direct and stepwise mechanisms for the zeolite-catalyzed benzene methylation. b) The different collective variables used for the sampling of the benzene methylation reaction.

C–O bond cleavage, one for the formation of a C–C bond between the methyl group and benzene, and one for the formation of an intermediate methoxide on the framework. Performing the simulation only with CN1 and CN2 (Figure 7), as was performed earlier in reference [44] for benzene methylation in H-ZSM-5, resulted in incomplete information. This could be related to the sampling of a third free energy minimum corresponding with an intermediate methoxide species, which was not captured by the selected CVs (the Supporting Information, Figure S10.1). To properly map the free energy landscape including transitions involving the methoxide intermediate, we thus opt to introduce the third collective variable (CN3 in Figure 7 b). This provides information on the competition between the two paths leading to the formation of a toluenium cation and water in H-SSZ-24 in one single simulation. A total simulation time of 235 ps was required to spawn 9422 hills (more details in the Computational Details and Section S11 of the Supporting Information).

After performing the MTD simulation and reconstructing the FES, a free energy in terms of three CVs is obtained. The sampling points and two free energy isosurfaces are displayed in Figure 8. Each dot indicates the position of the MTD walker

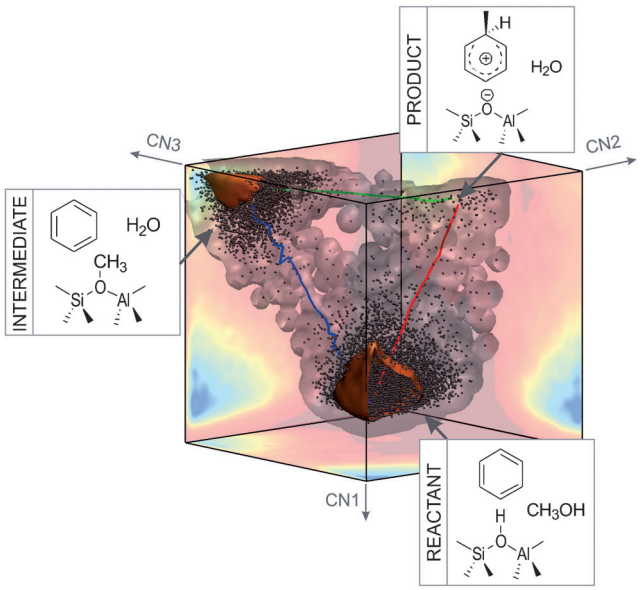

Figure 8. Isosurfaces at −0.1 (gray) and −10 kJ mol^{-1} (orange) of the FES obtained from the 235 ps metadynamics simulation of benzene methylation with two methanol molecules in H-SSZ-24 at 350 °C with 3 CVs. In the background, the 2D projections of the free energy surface are displayed. Additionally, the corresponding lowest free energy paths for the direct methylation (red) and stepwise methylation (blue and green) are shown.

after every 25 fs in the coarse-grained three dimensional collective variables space. On these positions the Gaussian hills are added, which, after summation, yield a reconstruction of the free energy surface. The resulting sampled paths are displayed in Figure S12.1 and Figure S12.2 (the Supporting Information). Figure 8 also displays two free energy isosurfaces on which the location of the three free energy minima can be distinguished: Methanol and benzene in the reactant well, water, benzene and a methoxide in an intermediate well, and a toluenium cation and water molecule in the product well. As methanol protonation occurs spontaneously at 350 °C as discussed earlier, the reactant well consists of both physisorbed and protonated methanol (the Supporting Information, Figure S13.1). As such, it can be assumed that the protonation step does not substantially contribute to the free energy barriers for methylation or methoxide formation. Hence, direct methylation or methoxide formation will only occur when there is enough energy available to break the methanol C–O bond. During the 235 ps simulation, transitions between all wells were sampled.

It should be noted that the free energy valleys corresponding with the transitions are relatively broad. This indicates that the same chemical transformation proceeds through a range of geometrically different pathways (the Supporting Information, Figure S12.1). Due to the significant probability of methanol protonation prior to reaction and the large available space in the AFI channels, the orientation of the reactants within the channel and with respect to the active site is rather free. This is translated in broad free energy minima and transition regions in the free energy surface. This observation further motivates the dynamical approach, taking into account more than one reactant, transition, and product state.

Some relevant snapshots of transitions are displayed in Figure 9, indicating that a wide variety of transition paths describe the same overall chemical reaction. From snapshots a, b, and c for the concerted methylation in Figure 9, it can be concluded that both single protonated methanol molecules (b,c) as protonated methanol dimers (a) can be part of the pre-reactive complex. As mentioned earlier, the probability to find methanol in a dimer conformation in the reactant well is 82%. During the 235 ps MTD simulation, the probability for methanol–methanol or methanol–water interactions is only 43%, indicating that after reaction and thus charge transfer to the hydrocarbon, the probability to form dimers of protic molecules is significantly lower (the Supporting Information, Figure S14.1). Also for the methoxide formation, the guest molecules can adopt many different configurations, leading to the sampling of many different transition states (Figure 9d and e).

To obtain chemical insight, one must be able to project all relevant information of this three-dimensional simulation onto a lower dimensional coordinate. This is not trivial and the technique we used earlier is no longer applicable.[42,44] Thus, a more flexible and universal tool is needed to project the obtained multidimensional free energy surface onto a lower dimensional reaction coordinate. Therefore, the lowest free energy path (LFEP) method proposed by Ensing and co-workers and implemented in the trace-irc program has been applied.[88] Hereby, a path connecting two free energy minima is constructed along the valley of lowest free energy. Figure 8 displays the calculated LFPEs for the direct methylation (red), methoxide formation (blue), and indirect methylation reaction (green). The one dimensional free energy profiles corresponding with these LFEPs are shown in Figure S15.1 (the Supporting Information) and the resulting free energy barriers and reaction free energies are summarized in Table 1. Convergence of the free energy profiles was achieved by simulating for a sufficiently long time and reducing the Gaussian hill height after barrier recrossings. All LFEPs were converged after the 235 ps simulation, as the profiles vary less than 5 kJ mol^{-1} during the last picoseconds of the simulation (the Supporting Information, Figure S15, 2, 3, 4). Note that for transitions to the products, no reaction free energy value is available because the product region is not entirely sampled to enhance multiple barrier crossings by introducing a wall in the MTD simulation (the Supporting Information, Section S11). From Table 1 we can conclude that under the given conditions, the direct and stepwise mechanisms are competing pathways, because both exhibit similar free energy barriers. Furthermore, it seems that the breaking of the C–O bond is the rate-limiting step during the direct methylation or methoxide formation because both reaction steps exhibit a nearly identical barrier. Recently, some of the present authors reported the free energy barrier of 122 kJ mol^{-1} for direct methylation of benzene in H-ZSM-5 with 2 methanol molecules at

Table 1. Free energy barrier and reaction free energy in kJ mol^{-1} for the direct and stepwise methylation of benzene in H-SSZ-24 by 2 methanol molecules at 350 °C.

	$\Delta G^{\ddagger}$ [kJ mol^{-1}]	ΔG_r [kJ mol^{-1}]
direct (R–P)	137.9	–
step 1 (R–IM)	138.5	43.6
step 2 (IM–P)	93.2	–

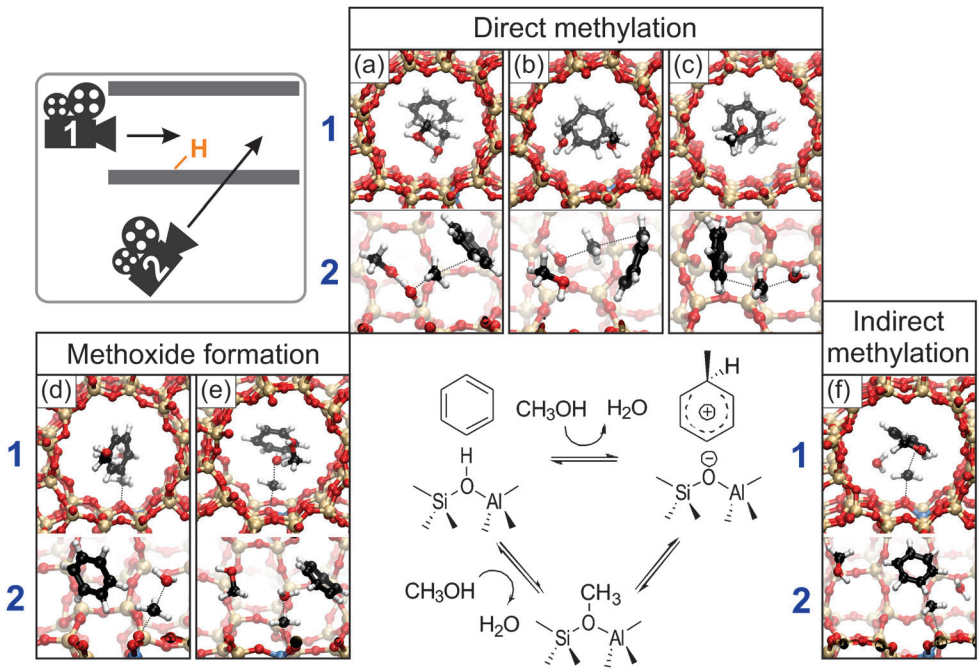

Figure 9. Snapshots of the direct (a,b,c) and stepwise methylation (d,e,f) of benzene by two methanol molecules in H-SSZ-24 at 350 °C, seen in the direction of the 1D channel (camera viewpoint 1) and in a cross section of the channel (camera viewpoint 2).

400 °C.[44] As it is expected that the acid strength of H-ZSM-5 and H-SSZ-24 are quite similar, this suggests that the large pores of H-SSZ-24 stabilize the transition states less efficiently than the medium pore sized H-ZSM-5. Similar observations were reported earlier for the methylation of benzene in H-ZSM-5 and H-Beta.[17]

The importance of surface methoxides and the stepwise methylation mechanism in general was recently underlined in several studies.[91–93] In a micro-kinetic modeling study based on DFT calculations and kinetic measurements, Brogaard et al. found that at typical methanol conversion conditions, the stepwise mechanism prevails for methylation of alkenes in the narrow pore material H-ZSM-22 due to the entropic benefit of intermediately releasing a water molecule.[91] A similar conclusion was recently made by Jones and Iglesia by using a kinetic, spectroscopic and theoretical study.[92] The authors stress that methoxy-mediated dissociative routes become dominant at certain conditions due to a delicate balance between entropic and enthalpic effects. These observations further underline that a study of various competitive pathways may certainly not be limited to the exploration of the PES at 0 K. A further in-depth discussion on the interplay of enthalpic and entropic effects may be found in the work of Gounder and Iglesia.[94]

Our second case study sheds light on the complexity, necessity, and usefulness of applying a multidimensional metadynamics approach to study elementary reaction steps in the MTO process for which different pathways may be competing. A purely static approach would not be sufficient for the material under study that exhibits wide channels, allowing many reactant and product configurations. Detailed mechanistic insights and a deeper understanding of the free energy surface of benzene methylation in H-SSZ-24 by two methanol molecules could be obtained. Some further insights can of course be obtained by complementing these simulations with other available molecular dynamics-based techniques, such as more advanced metadynamics simulations[37,95] or transition path sampling.[8] Depending on the system under investigation, the use of advanced molecular dynamics simulations may be necessary. However, they also come with a significant computational cost. Therefore, preliminary static calculations may reveal the necessity of molecular dynamics-based techniques as was done for methanol and benzene in H-SSZ-24 in reference [43].

Conclusion

Molecular dynamics simulations have proven their indispensable role in fields such as homogeneous catalysis for reactions in organic solvents and biochemistry for studies on protein folding. Within the field of catalysis, first principle molecular dynamics simulations of reactions are currently not widely applied. By using two case studies we have shown the potential of these techniques to mimic operating conditions while simulating chemical conversions. Indeed, by using such an approach, we were able to account for framework flexibility, the presence of additional guest molecules in the catalyst's pores and the existence of competitive pathways. The advantage of these methods relies on their ability to scan large portions of the potential and free energy surfaces. In the first case study, the effect of loading H-SAPO-34 at 350 °C with increasing amounts of protic guest molecules was investigated. The MD simulations with fully flexible unit cells revealed a significant expansion or contraction of the H-SAPO-34 framework upon adsorption of different amounts of methanol or water, respectively. In addition, proton mobility was observed and seemed to depend on the proton affinity of the adsorbed molecules, the loading of these molecules in the pores, and the mobility of the guest molecules. It might be important to take this highly dynamical phenomenon into account when protic molecules such as methanol or water are (co-)adsorbed in zeolitic materials. This effect can have important implications on the nature of the active site for zeolite conversions because chemical reactions do not necessarily take place at the Brønsted acid site, but can also occur near a protonated cluster of protic molecules in the pores of the material. In the second case study, the methylation of benzene in the presence of two methanol molecules at 350 °C in H-SSZ-24 was investigated. With this reaction we could demonstrate how competitive pathways, the presence of additional guest molecules in the pores, and the framework flexibility complicate the accurate sampling of a reaction. Because the framework is prone to deprotonation prior to reaction, any further reaction can start from physisorbed methanol, a single protonated methanol molecule, or a protonated methanol dimer. Moreover, the H-SSZ-24 material exhibits large pores, giving a large configurational freedom to the adsorbed molecules. Because of these two reasons, reactants can adopt many configurations, leading to a relatively flat potential energy surface. For this system, the metadynamics approach captures the complexity of the process adequately by probing a free energy surface spanned by three collective variables. After comparing the calculated lowest free energy paths, we concluded that the direct and stepwise methylation mechanisms are competing pathways in the AFI zeolite at 350 °C, because they exhibit nearly identical activation barriers. Moreover, due to the large available space in the large pore AFI material, there are multiple transition paths connecting the free energy minima. Indeed, in the calculated free energy surfaces broad transition regions were observed. The two presented cases nicely show the importance of approaches beyond a static methodology, focusing on one transition state. Furthermore, it is expected that the adopted dynamical methodology has a high potential for a variety of applications within zeolite catalysis.

Computational details

DFT simulations have been performed with the CP2K software package[96] by using the combined Gaussian and Plane Wave (GPW) basis sets approach.[97,98] The revPBE functional was chosen for its improved performance for solid-state calculations relative to the commonly used PBE functional.[99] The DZVP-GTH basis set and pseudopotentials[100] were used, and Grimme D3 dispersion corrections[101] were added. In the two case studies presented in this work, the silicoaluminophosphate H-SAPO-34 and aluminosilicate H-SSZ-24 are considered (see Figure 1). The H-SAPO-34 unit cell

contains 110 atoms and 2 acid sites, each consisting of a Si substitutional defect and a charge compensating proton (the Supporting Information, Figure S1.1). The H-SSZ-24 unit cell is relatively small, thus a $1\times1\times2$ super cell containing 145 atoms was used (the Supporting Information, Figure S8.1). The super cell contains one Al substitutional defect and thus one Brønsted acid site.

Ab initio molecular dynamics

In the two case studies, the behavior of guest molecules at 350 °C in H-SAPO-34 and H-SSZ-24 is assessed by ab initio molecular dynamics simulations. To fully account for the flexibility of the zeolite host and the dynamics of the guest molecules, the simulations were performed in the NPT ensemble at 350 °C and 1 bar. The resulting time-averaged cell parameters are summarized in Tables S1.1 and S8.1 (the Supporting Information). The time step for integration of the equations of motion was set to 0.5 fs. The system was equilibrated for 5 ps, followed by a production run of 50 ps. Because of the high computational demand of AIMD simulations, the simulation times are relatively short. As proton transfers are studied, first principle-based methods, rather than classical force fields, have to be applied. So far, there is only one molecular dynamics study reporting results on MTO reactions in H-ZSM-5 that uses the ReaxFF force field.[102]

The temperature was controlled by a chain of five Nosé–Hoover thermostats,[85] the pressure by an MTK barostat.[103] For reactions involving light atoms, nuclear quantum effects might become important. Nonetheless, the methodology applied to study proton mobility relies on classical equations of motion. The path integral formalism is very promising from this perspective, but further investigation and extensive testing in combination with quantum mechanical MD simulation packages is required.[104]

Metadynamics

In the second case study, the reactivity of benzene and two methanol molecules in H-SSZ-24 is assessed by using the metadynamics approach at 350 °C, a realistic MTO temperature, in the NVT ensemble. The temperature during the simulations is controlled by a chain of five Nosé–Hoover thermostats. During the actual MTD simulations, Gaussian hills are spawned along the collective variables (CV), defined by coordination numbers (CN):

$$CN = \sum_{i,j} \frac{1-(r_{ij}/r_0)^{nn}}{1-(r_{ij}/r_0)^{nd}} \qquad (3)$$

in which the sum runs over two sets of atoms i and j, r_{ij} is the distance between atoms i and j, and r_0 represents the reference distance. For all coordination numbers used in this study, a reference distance r_0 of 2.0 Å was chosen, because this value lies in the range of typical transition state distances of the bonds that have to be broken and formed during a methylation or methoxide formation. The parameters nn and nd are set to 6 and 12, respectively. With these coordination numbers as switch functions defining the order parameters, unbounded states are mapped on values close to zero, transition states on values around 0.5, and fully bonded states on values around 1. Quadratic walls were used to restrict the exploration of the FES to a particular area of interest (the Supporting Information, Section S11). The reacting methanol molecule is kept close to the acidic proton and the product valley is not entirely sampled to prevent the formation of more stable toluenium cations and as such enhance barrier recrossings (more details in the Supporting Information, Section S11). After the first and second recrossing of the transition point, the hill height is adequately halved to enhance the FES convergence. A new hill was spawned every 50 time steps. The width of all Gaussians was set to 0.02. The integration time step was set to 0.5 fs for all MTD simulations. To obtain one-dimensional free energy profiles from the reconstructed FES, the lowest free energy path was calculated according to reference [88]. Given the free energy profile, a free energy barrier $\Delta G^{\ddagger}$ is conveniently computed with Equation (2). Note that the calculation of separate enthalpic and entropic contributions require a different approach because these are slowly converging properties.[105] To compare the static and dynamic approach to describe a reaction, a transition state was localized using the dimer method implemented in CP2K.[106] A normal mode analysis was performed to confirm that the optimized transition state is a true first-order saddle point. To determine the pre-reactive complex and products, the intrinsic reaction coordinate was followed.

Acknowledgements

K.D.W. is a Ph.D. fellow funded by the Foundation of Scientific Research–Flanders (FWO) and received a FWO travel grant for his research stay at the van 't Hoff Institute for Molecular Sciences at University of Amsterdam. We are grateful to the Research Board of Ghent University and BELSPO in the frame of IAP P7/05. V.V.S. acknowledges funding from the European Research Council under the European Community's Seventh Framework Programme (FP7(2007-2013) ERC grant agreement number 240483), and from the European Union's Horizon 2020 research and innovation programme (consolidator ERC grant agreement No 647755–DYNPOR (2015–2020)). Computational resources and services used in this work were provided by the Stevin Supercomputer Infrastructure of Ghent University and by the VSC (Flemish Supercomputer Center), funded by the Hercules Foundation and the Flemish Government–department EWI. This work is part of the research program of the "Stichting voor Fundamenteel Onderzoek der Materie" (FOM), which is financially supported by the "Nederlandse Organisatie voor Wetenschappelijk Onderzoek" (NWO). We would like to thank U. Olsbye, S. Svelle and M. WestgårdErichsen (in GAP Center of Research Based Innovation, Department of Chemistry, University of Oslo) for fruitful discussions.

Keywords: ab initio calculations · heterogeneous catalysis · molecular dynamics · olefins · zeolites

[1] M. Guisnet, J. P. Gilson, *Zeolites for Cleaner Technologies, Vol. 3*, Imperial College Press, London, **2002**.
[2] W. Vermeiren, J. P. Gilson, *Top. Catal.* **2009**, *52*, 1131.
[3] B. Yilmaz, U. Muller, *Top. Catal.* **2009**, *52*, 888.
[4] M. Stöcker, *Microporous Mesoporous Mater.* **1999**, *29*, 3.
[5] U. Olsbye, S. Svelle, M. Bjørgen, P. Beato, T. V. W. Janssens, F. Joensen, S. Bordiga, K. P. Lillerud, *Angew. Chem. Int. Ed.* **2012**, *51*, 5810; *Angew. Chem.* **2012**, *124*, 5910.
[6] K. Hemelsoet, J. Van der Mynsbrugge, K. De Wispelaere, M. Waroquier, V. Van Speybroeck, *ChemPhysChem* **2013**, *14*, 1526.
[7] S. Ilias, A. Bhan, *ACS Catal.* **2013**, *3*, 18.
[8] V. Van Speybroeck, K. De Wispelaere, J. Van der Mynsbrugge, M. Vandichel, K. Hemelsoet, M. Waroquier, *Chem. Soc. Rev.* **2014**, *43*, 7326.
[9] I. M. Dahl, S. Kolboe, *J. Catal.* **1994**, *149*, 458.
[10] D. Lesthaeghe, V. Van Speybroeck, G. B. Marin, M. Waroquier, *Angew. Chem. Int. Ed.* **2006**, *45*, 1714; *Angew. Chem.* **2006**, *118*, 1746.

[11] W. G. Song, D. M. Marcus, H. Fu, J. O. Ehresmann, J. F. Haw, *J. Am. Chem. Soc.* **2002**, *124*, 3844.
[12] S. Svelle, F. Joensen, J. Nerlov, U. Olsbye, K. P. Lillerud, S. Kolboe, M. Bjorgen, *J. Am. Chem. Soc.* **2006**, *128*, 14770.
[13] M. Westgård Erichsen, S. Svelle, U. Olsbye, *Catal. Today* **2013**, *215*, 216.
[14] M. Westgård Erichsen, S. Svelle, U. Olsbye, *J. Catal.* **2013**, *298*, 94.
[15] S. Svelle, C. Tuma, X. Rozanska, T. Kerber, J. Sauer, *J. Am. Chem. Soc.* **2009**, *131*, 816.
[16] V. Van Speybroeck, J. Van der Mynsbrugge, M. Vandichel, K. Hemelsoet, D. Lesthaeghe, A. Ghysels, G. B. Marin, M. Waroquier, *J. Am. Chem. Soc.* **2011**, *133*, 888.
[17] J. Van der Mynsbrugge, M. Visur, U. Olsbye, P. Beato, M. Bjørgen, V. Van Speybroeck, S. Svelle, *J. Catal.* **2012**, *292*, 201.
[18] B. M. Weckhuysen, *Angew. Chem. Int. Ed.* **2009**, *48*, 4910; *Angew. Chem.* **2009**, *121*, 5008.
[19] P. M. Zimmerman, D. C. Tranca, J. Gomes, D. S. Lambrecht, M. Head-Gordon, A. T. Bell, *J. Am. Chem. Soc.* **2012**, *134*, 19468.
[20] J. Gomes, M. Head-Gordon, A. T. Bell, *J. Phys. Chem. C* **2014**, *118*, 21409.
[21] V. Kapko, C. Dawson, M. M. J. Treacy, M. F. Thorpe, *Phys. Chem. Chem. Phys.* **2010**, *12*, 8531.
[22] R. M. Barrer, D. E. W. Vaughan, *J. Phys. Chem. Solids* **1971**, *32*, 731.
[23] N. E. R. Zimmermann, S. Jakobtorweihen, E. Beerdsen, B. Smit, F. J. Keil, *J. Phys. Chem. C* **2007**, *111*, 17370.
[24] K. Hemelsoet, Q. Qian, T. De Meyer, K. De Wispelaere, B. De Sterck, B. M. Weckhuysen, M. Waroquier, V. Van Speybroeck, *Chem. Eur. J.* **2013**, *19*, 16595.
[25] J. Q. Chen, A. Bozzano, B. Glover, T. Fuglerud, S. Kvisle, *Catal. Today* **2005**, *106*, 103.
[26] S. Svelle, M. Visur, U. Olsbye, Saepurahman, M. Bjørgen, *Top. Catal.* **2011**, *54*, 897.
[27] E. A. Carter, G. Ciccotti, J. T. Hynes, R. Kapral, *Chem. Phys. Lett.* **1989**, *156*, 472.
[28] P. A. Bash, U. C. Singh, F. K. Brown, R. Langridge, P. A. Kollman, *Science* **1987**, *235*, 574.
[29] T. Huber, A. E. Torda, W. F. Vangunsteren, *J. Comput.-Aided Mol. Des.* **1994**, *8*, 695.
[30] J. R. Gullingsrud, R. Braun, K. Schulten, *J. Comput. Phys.* **1999**, *151*, 190.
[31] C. Jarzynski, *Phys. Rev. Lett.* **1997**, *78*, 2690.
[32] E. Darve, A. Pohorille, *J. Chem. Phys.* **2001**, *115*, 9169.
[33] L. Rosso, P. Minary, Z. W. Zhu, M. E. Tuckerman, *J. Chem. Phys.* **2002**, *116*, 4389.
[34] A. Laio, M. Parrinello, *Natl. Acad. Sci. USA* **2002**, *99*, 12562.
[35] M. Iannuzzi, A. Laio, M. Parrinello, *Phys. Rev. Lett.* **2003**, *90*, 4.
[36] D. Branduardi, F. L. Gervasio, M. Parrinello, *J. Chem. Phys.* **2007**, *126*, 054103.
[37] L. Sutto, S. Marsili, F. L. Gervasio, *Wiley Interdiscip. Rev.-Comput. Mol. Sci.* **2012**, *2*, 771.
[38] L. Benco, T. Bučko, J. Hafner, *J. Catal.* **2011**, *277*, 104.
[39] T. Bučko, L. Benco, J. Hafner, J. G. Angyan, *J. Catal.* **2011**, *279*, 220.
[40] T. Bučko, L. Benco, O. Dubay, C. Dellago, J. Hafner, *J. Chem. Phys.* **2009**, *131*, 11.
[41] T. Bučko, L. Benco, J. Hafner, J. G. Angyan, *J. Catal.* **2007**, *250*, 171.
[42] J. Van der Mynsbrugge, S. L. C. Moors, K. De Wispelaere, V. Van Speybroeck, *ChemCatChem* **2014**, *6*, 1906.
[43] M. Westgård Erichsen, K. De Wispelaere, K. Hemelsoet, S. L. C. Moors, T. Deconinck, M. Waroquier, S. Svelle, V. Van Speybroeck, U. Olsbye, *J. Catal.* **2015**; DOI: 10.1016/j.jcat.2015.01.013.
[44] S. L. C. Moors, K. De Wispelaere, J. Van der Mynsbrugge, M. Waroquier, V. Van Speybroeck, *ACS Catal.* **2013**, *3*, 2556.
[45] Q. Qian, J. Ruiz-Martínez, M. Mokhtar, A. M. Asiri, S. A. Al-Thabaiti, S. N. Basahel, B. M. Weckhuysen, *Catal. Today* **2014**, *226*, 14.
[46] V. Van Speybroeck, K. Hemelsoet, K. De Wispelaere, Q. Qian, J. Van der Mynsbrugge, B. De Sterck, B. M. Weckhuysen, M. Waroquier, *ChemCatChem* **2013**, *5*, 173.
[47] W. G. Song, J. F. Haw, J. B. Nicholas, C. S. Heneghan, *J. Am. Chem. Soc.* **2000**, *122*, 10726.
[48] B. Arstad, S. Kolboe, *J. Am. Chem. Soc.* **2001**, *123*, 8137.
[49] Database of zeolite structures: http://www.iza-structure.org/databases/.
[50] S. Bordiga, L. Regli, C. Lamberti, A. Zecchina, M. Bjørgen, K. P. Lillerud, *J. Phys. Chem. B* **2005**, *109*, 7724.
[51] J. Limtrakul, P. Chuichay, S. Nokbin, *J. Mol. Struct.* **2001**, *560*, 169.
[52] I. Stich, J. D. Gale, K. Terakura, M. C. Payne, *Chem. Phys. Lett.* **1998**, *283*, 402.
[53] V. V. Mihaleva, R. A. van Santen, A. P. J. Jansen, *J. Phys. Chem. B* **2001**, *105*, 6874.
[54] L. Smith, A. K. Cheetham, R. E. Morris, L. Marchese, J. M. Thomas, P. A. Wright, J. Chen, *Science* **1996**, *271*, 799.
[55] V. Termath, F. Haase, J. Sauer, J. Hutter, M. Parrinello, *J. Am. Chem. Soc.* **1998**, *120*, 8512.
[56] M. V. Vener, X. Rozanska, J. Sauer, *Phys. Chem. Chem. Phys.* **2009**, *11*, 1702.
[57] H. Huo, L. M. Peng, C. P. Grey, *J. Phys. Chem. C* **2009**, *113*, 8211.
[58] J. D. Gale, R. Shah, M. C. Payne, I. Stich, K. Terakura, *Catal. Today* **1999**, *50*, 525.
[59] F. Haase, J. Sauer, J. Hutter, *Chem. Phys. Lett.* **1997**, *266*, 397.
[60] L. Marchese, J. S. Chen, P. A. Wright, J. M. Thomas, *J. Phys. Chem.* **1993**, *97*, 8109.
[61] M. Krossner, J. Sauer, *J. Phys. Chem.* **1996**, *100*, 6199.
[62] P. D. Caesar, R. A. Morrison, Mobil Oil Corporation (New York, NY), US Patent number US4083889, United States, **1978**.
[63] D. Seddon, T. Mole, J. A. Whiteside, Imperial Chemical Industries PLC (London, GB2), US Patent number US4499314, United States, **1985**.
[64] P. Tschaufeser, S. C. Parker, *J. Phys. Chem.* **1995**, *99*, 10609.
[65] M. Amri, R. I. Walton, *Chem. Mater.* **2009**, *21*, 3380.
[66] D. S. Wragg, R. E. Johnsen, P. Norby, H. Fjellvåg, *Microporous Mesoporous Mater.* **2010**, *134*, 210.
[67] D. S. Wragg, R. E. Johnsen, M. Balasundaram, P. Norby, H. Fjellvåg, A. Gronvold, T. Fuglerud, J. Hafizovic, O. B. Vistad, D. Akporiaye, *J. Catal.* **2009**, *268*, 290.
[68] M. Zokaie, D. S. Wragg, A. Gronvold, T. Fuglerud, J. H. Cavka, K. P. Lillerud, O. Swang, *Microporous Mesoporous Mater.* **2013**, *165*, 1.
[69] D. S. Wragg, M. G. O. Brien, F. L. Bleken, M. Di Michiel, U. Olsbye, H. Fjellvåg, *Angew. Chem. Int. Ed.* **2012**, *51*, 7956; *Angew. Chem.* **2012**, *124*, 8080.
[70] R. V. Awati, P. I. Ravikovitch, D. S. Sholl, *J. Phys. Chem. C* **2013**, *117*, 13462.
[71] A. Alberti, A. Martucci, *J. Phys. Chem. C* **2010**, *114*, 7767.
[72] J. Kanellopoulos, C. Gottert, D. Schneider, B. Knorr, D. Prager, H. Ernst, D. Freude, *J. Catal.* **2008**, *255*, 68.
[73] J. A. Ryder, A. K. Chakraborty, A. T. Bell, *J. Phys. Chem. B* **2000**, *104*, 6998.
[74] K. De Wispelaere, K. Hemelsoet, M. Waroquier, V. Van Speybroeck, *J. Catal.* **2013**, *305*, 76.
[75] A. Pavlova, E. J. Meijer, *ChemPhysChem* **2012**, *13*, 3492.
[76] R. Krishna, J. M. van Baten, *Langmuir* **2010**, *26*, 10854.
[77] W. L. Jolly, *Modern Inorganic Chemistry*, 2nd ed., McGraw-Hill College, New York, **1991**.
[78] K. D. Kreuer, *Chem. Mater.* **1996**, *8*, 610.
[79] A. Hassanali, F. Giberti, J. r. m. Cuny, T. D. Kühne, M. Parrinello, *Proc. Natl. Acad. Sci. USA* **2013**, *110*, 13723.
[80] A. F. Combariza, G. Sastre, A. Corma, *J. Phys. Chem. C* **2011**, *115*, 875.
[81] G. Sastre, *Catal. Today* **2014**, *226*, 25.
[82] D. Lesthaeghe, B. De Sterck, V. Van Speybroeck, G. B. Marin, M. Waroquier, *Angew. Chem. Int. Ed.* **2007**, *46*, 1311; *Angew. Chem.* **2007**, *119*, 1333.
[83] I. Hill, A. Malek, A. Bhan, *ACS Catal.* **2013**, *3*, 1992.
[84] D. M. McCann, D. Lesthaeghe, P. W. Kletnieks, D. R. Guenther, M. J. Hayman, V. Van Speybroeck, M. Waroquier, J. F. Haw, *Angew. Chem. Int. Ed.* **2008**, *47*, 5179; *Angew. Chem.* **2008**, *120*, 5257.
[85] D. Frenkel, B. Smit, *Understanding Molecular Simulations*, 2nd ed., Academic Press, San Diego, **2002**.
[86] C. Abrams, G. Bussi, *Entropy* **2013**, *16*, 163.
[87] A. Laio, A. Rodriguez-Fortea, F. L. Gervasio, M. Ceccarelli, M. Parrinello, *J. Phys. Chem. B* **2005**, *109*, 6714.
[88] B. Ensing, A. Laio, M. Parrinello, M. L. Klein, *J. Phys. Chem. B* **2005**, *109*, 6676.
[89] A. Laio, F. L. Gervasio, *Rep. Prog. Phys.* **2008**, *71*, 126601.
[90] A. Barducci, M. Bonomi, M. Parrinello, *Wiley Interdiscip. Rev.-Comput. Mol. Sci.* **2011**, *1*, 826.

[91] R. Y. Brogaard, R. Henry, Y. Schuurman, A. J. Medford, P. G. Moses, P. Beato, S. Svelle, J. K. Nørskov, U. Olsbye, *J. Catal.* **2014**, *314*, 159.
[92] A. J. Jones, E. Iglesia, *Angew. Chem. Int. Ed.* **2014**, *53*, 12177.
[93] J. Van der Mynsbrugge, J. De Ridder, K. Hemelsoet, M. Waroquier, V. Van Speybroeck, *Chem. Eur. J.* **2013**, *19*, 11568.
[94] R. Gounder, E. Iglesia, *Acc. Chem. Res.* **2012**, *45*, 229.
[95] G. D. Leines, B. Ensing, *Phys. Rev. Lett.* **2012**, *109*, 4.
[96] J. VandeVondele, M. Krack, F. Mohamed, M. Parrinello, T. Chassaing, J. Hutter, *Comput. Phys. Commun.* **2005**, *167*, 103.
[97] G. Lippert, J. Hutter, M. Parrinello, *Theor. Chem. Acc.* **1999**, *103*, 124.
[98] G. Lippert, J. Hutter, M. Parrinello, *Mol. Phys.* **1997**, *92*, 477.
[99] K. Yang, J. J. Zheng, Y. Zhao, D. G. Truhlar, *J. Chem. Phys.* **2010**, *132*, 10.
[100] S. Goedecker, M. Teter, J. Hutter, *Phys. Rev. B* **1996**, *54*, 1703.
[101] S. Grimme, J. Antony, S. Ehrlich, H. Krieg, *J. Chem. Phys.* **2010**, *132*, 154104.
[102] C. Bai, L. C. Liu, H. Sun, *J. Phys. Chem. C* **2012**, *116*, 7029.
[103] G. J. Martyna, D. J. Tobias, M. L. Klein, *J. Chem. Phys.* **1994**, *101*, 4177.
[104] M. Ceriotti, J. More, D. E. Manolopoulos, *Comput. Phys. Commun.* **2014**, *185*, 1019.
[105] C. Michel, A. Laio, A. Milet, *J. Chem. Theory Comput.* **2009**, *5*, 2193.
[106] G. Henkelman, H. Jónsson, *J. Chem. Phys.* **1999**, *111*, 7010.

Received: February 5, 2015
Published online on ■■ ■■, 2015

FULL PAPER

Unravelling zeolite catalysis: The potential and free energy surface of zeolite-catalyzed reactions at real operating conditions can be complex. As such, techniques that allow sampling of larger portions of the potential and free energy landscape are required to obtain accurate information. By means of two case studies, the potential of advanced molecular dynamics simulations is demonstrated to study the complex and highly dynamical behavior within zeolite catalysis (see figure).

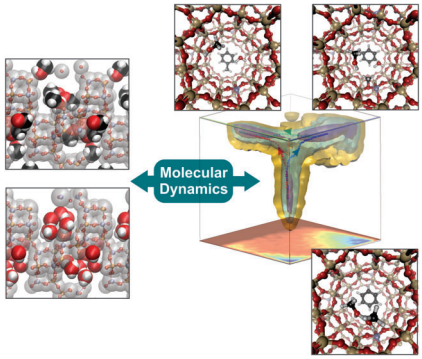

Molecular Dynamics

K. De Wispelaere, B. Ensing, A. Ghysels, E. J. Meijer, V. Van Speybroeck**

■■ – ■■

Complex Reaction Environments and Competing Reaction Mechanisms in Zeolite Catalysis: Insights from Advanced Molecular Dynamics

The free energy surface.....of zeolite-catalyzed reactions at real operating conditions is typically complex. As such, techniques that allow sampling of larger portions of the potential and free energy landscape are required to mimic experimental conditions as closely as possible. Various points on the free energy surface can be connected by a multitude of reaction paths. Mapping the free energy surface by advanced molecular dynamics simulations of a zeolite-catalyzed reaction can hence be compared with studying a map in an atlas to discover the possible means of transport to travel between two cities. For the complete story see the Full Paper on page ■■ ff. by B. Ensing, V. Van Speybroeck et al.